Photoionization of atomic oxygen at the multiplet term level from 20 to 212 eV

S. J. Schaphorst,[1,*] M. O. Krause,[2] C. D. Caldwell,[1] H. P. Saha,[1] M. Pahler,[1,†] and J. Jiménez-Mier[3]
[1]*Department of Physics, University of Central Florida, Orlando, Florida 32816-2385*
[2]*Oak Ridge National Laboratory, Oak Ridge, Tennessee 37831-6201*
[3]*Instituto de Ciencias Nucleares, Universidad Nacional Autónoma de México, 04510 México Distrito Federale, Mexico*
(Received 10 March 1995)

The valence shell photoionization branching ratios of atomic oxygen are measured at the multiplet term level in a synchrotron-radiation-based electron spectrometry experiment and calculated using the multiconfiguration Hartree-Fock (MCHF) method for photon energies between 20 and 212 eV. The $[2p]({}^4S,{}^2D,{}^2P)$ branching ratios, $[2s]^2P$ to $[2s]^4P$ intensity ratio, and $[2s]$ to $[2p]$ cross-section ratio for removal of a $2s$ or $2p$ electron are presented, and satisfactory agreement between the experiment and the MCHF calculation is found. In addition, the relative photoionization cross section is measured between 24 and 122 eV and is compared with calculations and a previous absolute cross-section measurement. Good agreement between the experimental and MCHF results is seen.

PACS number(s): 32.80.Fb

I. INTRODUCTION

While a detailed understanding of the photoionization process in closed-shell atoms has emerged [1–4] following the first studies at the subshell level [5–7], a corresponding understanding of open-shell atoms has yet to evolve. The photoionization of open-shell atoms leads to a multiplet of final LSJ ionic states due to the angular momentum coupling possibilities in the presence of an open subshell. Experimental methods such as electron spectrometry, which can differentiate the photoionization process at the LSJ term level, are particularly helpful in leading to an understanding of open-shell systems, but have been relatively rare [8–11] and generally limited to a narrow range of photon energy. Consequently, theoretical studies that have predicted dynamic properties in the photoionization of open-shell atoms, from calculations performed in the 1960's and 1970's to recent more sophisticated calculations, have remained largely untested by experiment, even though the results of the calculations have often been at variance with one another.

Of primary interest are the relative photoionization cross sections for LSJ terms of a particular nl subshell. Under the assumptions that correlations in the initial and final states of the system are negligible and that transition amplitudes are independent of the final ionic state, these branching ratios are expected to be constant and purely geometric, thereby determined solely by the angular momentum coupling of the relevant transition states [12–14]. Dynamic effects, such as those associated with a term dependence of the transition matrix elements, can cause deviations from purely geometric values. Approaching threshold, in addition to dynamic effects, kinetic effects arising from the different binding energies of the final LSJ ionic states in combination with a slope in the cross section might also be expected to cause such deviations in the relative cross sections.

Several experiments performed on halogen atoms [11,15–18] with photon energies 5–20 eV above the valence subshell thresholds have found branching ratios for the LSJ terms to be surprisingly close to the geometric values. Similarly, studies of the atomic oxygen $2p$ subshell branching ratios with photon energies ranging from close to threshold to 25 eV, which employed He I [19] or synchrotron [9,20] radiation, and above the $2s\rightarrow np$ autoionization resonances at 40.8 eV [21], have indicated that these ratios do not deviate strongly from the geometric values. However, a measurement of the branching ratios for an open-shell atom over a broad energy range which is free of Cooper minima and autoionization resonances is still lacking.

Atomic oxygen represents a particularly good test case for the influence of dynamic effects on the branching ratios over a wide range of photon energy, as it possesses a relatively simple electronic structure and lacks a Cooper minimum. Moreover, the results of such a study will provide detailed information for the modeling of physical and chemical processes in the upper atmosphere, where atomic oxygen is one of the major constituents. Previously, cross-section data have been drawn mostly from calculations and a few experimental data of limited scope, as summarized in the latest compilations [22,23].

We present measured and calculated branching ratios for photoionization from the open $2p$ and closed $2s$ subshells of atomic oxygen in the photon energy region $20\leqslant h\nu\leqslant 212$ eV. The experimental results are compared with a multiconfiguration Hartree-Fock (MCHF) calculation, geometric values based on an LS coupling scheme, and with the most relevant experimental [9,19–21] and theoretical [24–28] results. The relative total cross sections for all one-electron processes between 24 and 122 eV are also determined and compared with theory as well as an experiment in which the total ion yield was measured [29]. When combined with recent highly differentiated measurements in the energy region of autoionization resonances within the $2p$ manifold up to 29 eV [9] and

*Present address: Fakultät für Physik, Universität Freiburg, D-79104 Freiburg, Federal Republic of Germany.
†Present address: Fafnir GmbH, Bahrenfelder Strasse 19, D-22765 Hamburg, Federal Republic of Germany.

the photoexcited resonant and normal KLL Auger electron spectra [30–32], the present work provides a comprehensive account of the dominant photoexcitation and deexcitation processes for atomic oxygen between 15 and 600 eV.

II. EXPERIMENT

The experiment was performed at the Aladdin storage ring of the Synchrotron Radiation Center (SRC) in Stoughton, Wisconsin, using three different SRC monochromators: the 3-m toroidal grating monochromator (TGM) for the photon energy range 20–122 eV, the Mark V Grasshopper from 100 to 175 eV, and the 10-m TGM at 212 eV. The electron spectrometer and experimental setup have been described in detail elsewhere [9,33]. The system consists of three spherical sector plate analyzers mounted at right angles to one another on a platform that can be rotated about the direction of the ionizing radiation. The analyzers have a nominal resolution of $\Delta E/E = 0.01$ and for these measurements were operated with pass energies ranging from 10.0 to 50.0 eV for the best compromise between effective resolution in eV [full width at half maximum (FWHM)] and intensity. The effective photoelectron spectrometry (PES) resolution varied from 0.15 to 0.5 eV for photon energies from 20 to 120 eV and from 0.80 to 1.4 eV for photon energies from 125 to 175 eV and was 1.0 eV at a photon energy of 212 eV.

To avoid effects due to the angular dependence of the photoelectron intensity, measurements were made at the pseudo-magic angle $\theta_m = (1/2)\cos^{-1}(-1/3p)$ as referred to the major axis of the polarization ellipse. The degree of linear polarization p of the incident radiation and the symmetry of the source volume were monitored based on the angular distributions of rare gas photoelectron and Auger electron peaks with well-known angular distribution parameters β. The degree of linear polarization was measured to be, on the average, 82(2)% for the 3-m TGM low-energy grating, 72(3)% for the 3-m TGM high-energy grating, 82(1)% for the Mark V monochromator, and 79(3)% for the 10-m TGM. The polarization was found to have a slight photon energy dependence for each monochromator. The monochromators were calibrated in energy by determining the overlap of the Xe $5p$ photolines in first order and the Xe $4d$ photolines from second order radiation for the 3-m TGM, the K-shell absorption edge of a thin Be foil with a Fermi level of 112.00 eV [34] for the Mark V, and the overlap of the Ne $2p$ photoline with the O_2 K Auger line at 500.5 eV [35] for the 10-m TGM.

Oxygen atoms were produced in a 2.45-GHz microwave discharge from molecular oxygen of purity $>99.99\%$. The inner walls of the discharge tube were coated with phosphorous pentoxide to reduce the recombination rate on the surfaces. The molecular and atomic species flowed into the ionization region through an 11-mm-diam, 30-cm-long flow tube coated with halocarbon wax, with a 5-mm-diam flow restriction at the end to maintain a pressure gradient between the discharge tube and the scattering region. By adding a small amount of N_2 to the discharge, the atomic oxygen yield was seen to improve considerably, from about 25–30 % to typically 50–60 % [30]. In addition to atomic oxygen, the discharge produced small amounts of nitric oxide and the electronically excited $O_2\,^1\Delta_g$ state. The presence of these species complicated the background subtraction procedure.

Photoelectron spectra were normally recorded in the constant pass energy mode in which a staircase voltage is applied to the source cell, although some measurements in the constant retardation-acceleration mode in which the pass energy of the analyzer is varied were performed for consistency checks on the relative intensities. For the determination of the $[2p]({}^4S,{}^2D,{}^2P)$ branching ratios and the $[2s]^2P$ to $[2s]^4P$ cross-section ratio over the entire energy region up to 212 eV, the transmission function of the electron analyzer was calibrated using the relative cross-sections of the neon $2s$ and $2p$ photopeaks [7,36–38]. For measuring the photon energy dependence of the relative atomic oxygen $2p$ and $2s$ cross sections, the transmission functions of the 3-m TGM gratings were calibrated primarily using the known Ne $2p$ [36,38] cross section and, secondarily, using the relative cross sections of the ever-present $O_2\,^2\Pi_g$ [39] molecular contribution. No such calibrations of the transmission dependence were performed for the other monochromators; hence, the relative cross-section measurements extend only up to the 122-eV maximum energy of the 3-m TGM.

III. THEORY

A theoretical calculation was performed for the photoionization of the ground state of the oxygen atom using the multiconfiguration Hartree-Fock method, which, *inter alia*, has been quite successful in explaining the Auger spectra of atomic oxygen [31]. A systematic investigation of the partial cross section for production of each of the LS components of the final ionic states arising from removal of either a $2s$ or $2p$ electron has been made, i.e.,

$$h\nu + \mathrm{O}(2s^2 2p^4\,{}^3P) \rightarrow \mathrm{O}^+(2s^2 2p^3\,{}^4S,{}^2D,{}^2P) + e^- \rightarrow \mathrm{O}^+(2s2p^4\,{}^4P,{}^2D,{}^2S,{}^2P) + e^- . \quad (1)$$

The $1s$, $2s$, and $2p$ core orbitals were first obtained from the MCHF calculation of the two configurations $2s^2 2p^3({}^2P)$ and $2p^5({}^2P)$ of the oxygen ion, which mix strongly. To optimize the $1s$, $2s$, and $2p$ wave functions for each of the final ionic states, we performed a MCHF calculation for the configuration set consisting of $2s^2 2p^3({}^2D,{}^2P)3d\,{}^3P$ and $2s2p^4({}^4P,{}^2P,{}^2D)3p\,{}^3P$, varying the $2s$, $2p$, $3p$, and $3d$ orbitals to obtain consistent $2s$ and $2p$ wave functions for each state. The wave function for the $2s^2 2p^4({}^3P)$ ground state was then determined using these $1s$, $2s$, and $2p$ orbitals. In the calculation of the ground state, the MCHF expansion is represented as a bound state of the electron-plus-ion system, and all channels are retained which can be formed from these ionic configurations. Separate MCHF calculations were performed for each ionic state, keeping $1s$, $2s$, and $2p$ orbitals the same as before, and varying the additional $3s$, $3p$, and $3d$ excited orbitals. In this way the threshold energies for each of the ionic states were obtained, and they were found to be in very good agreement with experiment.

The final continuum state wave functions corresponding to each of the ionic states were determined using the MCHF method for continuum wave functions [40]. The MCHF expansion for the final continuum states consistent with proper

LS coupling and parity conservation includes a set of open channels and some excited bound configurations generated from the single and double replacement of the core ionic orbitals, which account for the electron correlation and polarization. The excited state orbitals were optimized along with the continuum in each of the final continuum states.

The bound and continuum orbitals obtained as described above for the separate *LS* final states corresponding to each of the ionic configurations were used along with the initial state wave functions to calculate the dipole matrix elements for the partial photoionization cross sections. The length and velocity forms of each of the partial cross sections are found to be in reasonably good agreement, as are those for the corresponding branching ratios for each of the various processes. The total cross sections have been calculated by summing over the partial cross sections, and in this case the length and velocity forms are also in satisfactory agreement.

IV. RESULTS AND DISCUSSION

The atomic oxygen photopeaks were extracted from "discharge-on" ("on") spectra by subtracting the spectra associated with the precursor molecule O_2, the additive N_2, and species created by the microwave discharge. The procedure is illustrated in Fig. 1. In Fig. 1(a) is shown an "on" spectrum recorded at a photon energy of 91.0 eV. Below the "on" spectrum are spectra of the O_2^+, N_2^+, and NO^+ molecules corresponding to the same photon energy. Normalization of the spectra relevant to each other for the purposes of the subtraction was performed at the features indicated by circles, asterisks, and lines.

"Discharge-off" ("off") spectra for N_2 were recorded individually for photon energies up to 122 eV and for O_2 at all photon energies. It should be noted at the O_2 spectra usually contained an admixture of N_2 which was, however, different in the "off" spectra from that in the "on" spectra. Above 122 eV the partial cross sections for the production of the N_2^+ bands were obtained by extrapolation and normalized to the $^2\Sigma_g^+$ peak, indicated with a line in Fig. 1(a). "off" spectra were not recorded directly for NO. However, for photon energies below approximately 70 eV, the PES resolution was sufficient to separate the NO^+ structure from the atomic oxygen photopeaks. The contributions of NO^+ to the "on" spectra at higher energies were determined by using the intensities of the well-isolated $X^1\Sigma^+$ and $C^3\Pi$ peaks marked by asterisks in Fig. 1(a) and applying the partial cross sections as measured in previous studies [41–44]. The NO^+ spectrum in Fig. 1(a) has been simulated on the basis of these partial cross sections.

Following the subtraction of the O_2^+, N_2^+, and NO^+ contributions from the "on" spectrum, there remains a background spectrum associated with the photoionization of the excited $O_2\,^1\Delta_g$ state labeled $^*O_2^+$ in Fig. 1(b). A higher-resolution spectrum recorded at 21.9 eV shown in Fig. 2 displays more clearly the main contributions from $^*O_2^+$ (and also from NO^+). The PES resolution for photon energies below approximately 120 eV permitted the $^*O_2^+$ contribution, which is small relative to the O $[2p]$ photopeaks, to be separated by a fitting procedure. The population of the metastable electronically excited $O_2\,^1\Delta_g$ state by a microwave discharge has been previously observed and studied

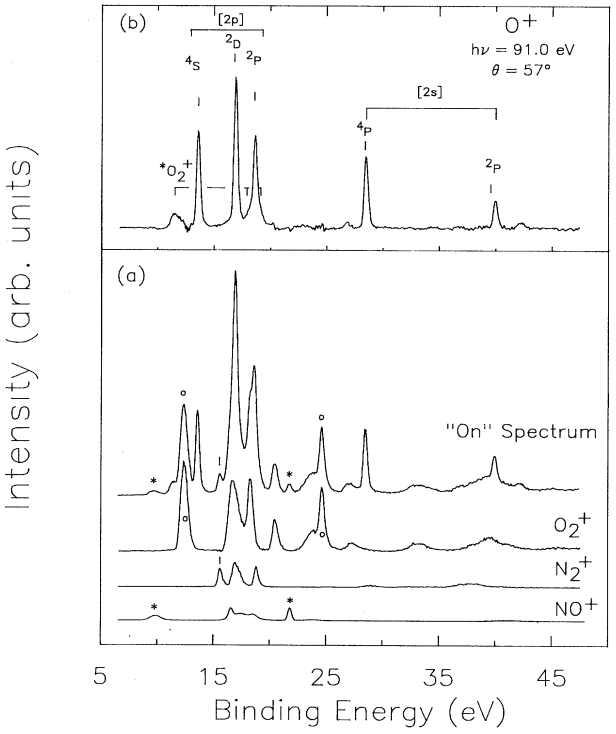

FIG. 1. Photoelectron spectrum of the oxygen atom recorded at a photon energy of 91.0 eV. (a) displays a "discharge-on" spectrum and the corresponding "discharge-off" spectra for the precursor molecule O_2 and the additive N_2. The NO molecule is created in the microwave discharge and the NO^+ spectrum is based on the partial cross sections from previous studies [41–44]. Symbols identify the peaks in the spectra in (a) used for the normalization in the subtraction procedure. (b) displays the resulting atomic oxygen spectrum with its $[2p]$ and $[2s]$ photopeaks in addition to the $^*O_2^+$ structure associated with the photoionization of the excited $O_2\,^1\Delta_g$ state. Each spectrum was recorded at the pseudo-magic angle and contains 512 channels.

[45–47]. We found that in the photon energy range from 70 to 120 eV, the intensities of the $^*O_2^+$ peaks between 16 and 20 eV relative to the $^2\Pi_g$ peak at 11.5 eV binding energy are by and large independent of photon energy. We maintained the constant spectral distribution of the $^*O_2^+$ structure at $h\nu > 120$ eV, where a direct identification of the overlapping $^*O_2^+$ peaks was no longer possible, and subtracted their contributions by normalizing to the well-isolated $^2\Pi_g$ peak.

The atomic oxygen photolines were fit with Pearson-7 functions, which approximate the Voigt line profile [48], although it should be noted that the contribution of the natural width to the total width for these spectra is negligible. The widths and shapes of the O^+ peaks were fixed to be the same in the fitting procedure, which is particularly advantageous in differentiating the $[2p]^2D$ and $[2p]^2P$ peaks from the underlying $^*O_2^+$ and NO^+ structure and any residuals in spectra recorded at higher photon energies. (We use the notation in which a square bracket indicates a vacancy in a subshell.) The intensities for the resulting atomic peaks obtained from the fitting procedure were corrected for the electron analyzer transmission function.

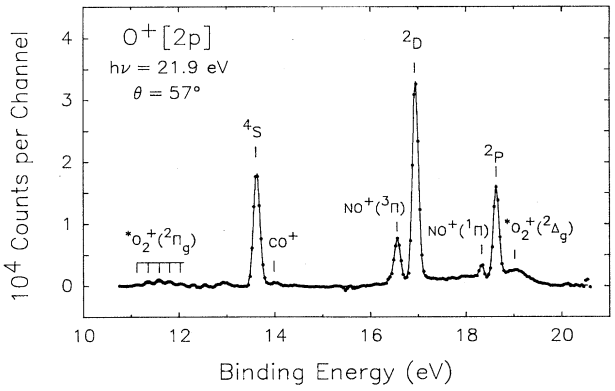

FIG. 2. Photoelectron spectrum of the atomic oxygen $[2p]$ final ionic states recorded at a photon energy of 21.9 eV, following the subtraction of the O_2^+ and N_2^+ components. Molecular products created by the discharge are identified. The solid line represents a χ^2 fit to the data. The spectrum consists of 256 channels.

The uncertainties in the intensities derive from (1) statistical uncertainty in the recorded intensities, (2) the uncertainty in the subtraction of the contributions from the molecular components, (3) the scatter between different measurements, and (4) the uncertainty in the transmission function correction for the analyzers. At the lower photon energies, the major uncertainty arises from the transmission function correction. At higher photon energies the major uncertainty arises from the background subtraction of the $^*O_2^+$ and NO^+ structure underlying the $[2p]^2D$ and ^2P peaks and the need to extrapolate in order to determine the relative intensities for the molecular bands.

A. Branching ratios for the $[2p]$ multiplets

The measured branching ratios for the $O^+[2p]^4S,^2D$, and ^2P multiplet lines are listed in Table I and compared in Fig. 3 with our MCHF calculation and the geometric values. The larger error bars for photon energies above about 100 eV reflect primarily the uncertainty in the molecular background underlying the ^2D and ^2P peaks. The branching ratios between 137 and 175 eV, measured with the Grasshopper, also suffer from a lower photon flux and a low PES resolution, which complicated the subtraction procedure. This could cause a possible systematic error that would increase with photon energy due to the increasingly lower resolution of the monochromator. Estimated to be smaller than the other uncertainties, this error was not included in the assessment of the overall uncertainty. The increased photon flux from the 10-m TGM permitted a higher-resolution spectrum to be recorded at 212 eV and led to the smaller errors at this photon energy. This spectrum is shown in Fig. 4.

For photon energies above the $2s \rightarrow np$ autoionization region ending at 40 eV, the experimental and MCHF $[2p]$ branching ratios agree satisfactorily regarding the magnitudes and energy dependences. However, the experimental data taken by themselves would allow for slight slopes within the error limits. While the experimental and MCHF branching ratios for the ^4S and ^2P ionic states agree well over the photon energy range from 35 to 125 eV, the experimental $[2p]^2D$ branching ratio decreases slowly between 40 and 212 eV, whereas the MCHF values show a very slight increase over this photon energy range. The measured and calculated ratios in this region lie close to the geometric values of 5/12, 1/3, and 1/4 for the $^2D,^4S$, and ^2P states, respectively [13]. The good agreement between the measured branching ratios and the geometric values at high photon energies indicates the relative accuracy of LS coupling and the single-configuration model [13] in describing the initial and final states, in addition to the expected independence of

TABLE I. Measured photoionization branching ratios for the atomic oxygen $[2p](^4S,^2D,^2P)$ final ionic states.

$h\nu$ (eV)	^4S	^2D	^2P
19.9	0.382(25)	0.466(25)	0.151(16)
21.9	0.337(19)	0.477(22)	0.186(16)
23.9	0.311(19)	0.476(21)	0.213(15)
34.9	0.290(15)	0.459(17)	0.252(14)
40.9	0.299(15)	0.460(17)	0.241(13)
44.9	0.299(15)	0.465(16)	0.236(12)
49.9	0.304(14)	0.452(16)	0.244(13)
60.4	0.318(13)	0.442(15)	0.240(12)
70.5	0.310(11)	0.450(13)	0.240(11)
80.8	0.311(12)	0.443(14)	0.246(10)
91.0	0.308(12)	0.441(14)	0.251(11)
100.0	0.323(19)	0.438(22)	0.240(20)
101.2	0.295(13)	0.425(15)	0.280(11)
111.4	0.307(13)	0.437(17)	0.256(12)
121.7	0.308(24)	0.459(34)	0.233(28)
125.0	0.330(24)	0.433(28)	0.237(27)
138.5	0.316(22)	0.413(23)	0.271(22)
150.0	0.310(23)	0.408(31)	0.282(28)
175.0	0.330(32)	0.378(44)	0.292(39)
212.0	0.352(26)	0.407(31)	0.241(26)

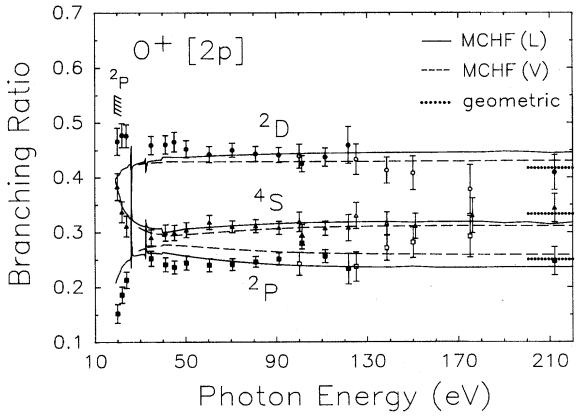

FIG. 3. Comparison of experimental and theoretical atomic oxygen $[2p]$ branching ratios. The MCHF length and velocity gauge results are indicated by solid and dashed lines, respectively. The geometric values are represented by the dotted lines. The $[2p]^2D,^4S$, and ^2P final ionic states are represented by circles, triangles, and squares, respectively, with measurements made on the Mark V monochromator indicated by open symbols.

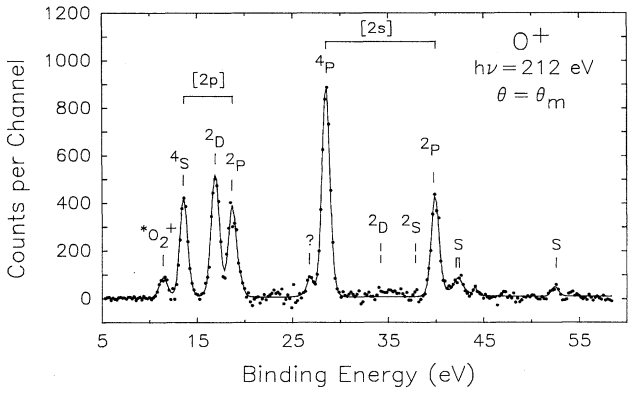

FIG. 4. Photoelectron spectrum of atomic oxygen recorded at a photon energy of 212 eV following the subtraction of the O_2^+, N_2^+, and NO^+ contributions. The solid line represents a χ^2 fit to the data. The spectrum consists of 256 channels and has not been corrected for transmission function effects of the electron spectrometer. Several correlation satellites (S) are marked, and the positions of the $[2s]^2D,^2S$ multiplet lines are indicated. The peak (?) at 26.8 eV may be due to excited O_2.

the transition matrix elements in the final ionic states. The apparent deviations of the experimental branching ratios between 137 and 175 eV, and to a lesser extent at 212 eV, from the essentially constant values might be attributed to the difficulties in subtracting the NO^+ and $*O_2^+$ structure at the resolution attainable in this range.

While our experimental work presents the only data over a wide photon energy range, several calculations exist which cover the energy range shown in Fig. 3. For the sake of clarity, these earlier theoretical results and the measurements of the $[2p]$ intensity ratios available below 41 eV are not included in the figure, but are compared with our results at selected photon energies in Table II. A comparison of the branching ratios in terms of the ^2D to ^4S and ^2P to ^4S cross-section ratios as shown in Table II is preferable close to threshold due to the relatively large uncertainty in the electron analyzer transmission function for electrons of low kinetic energy and the relative ease of establishing a reliable ^4S reference. The ratios predicted in an early close-coupling calculation [24] are seen to converge to the asymptotic geometric ratios by 95.0 eV but disagree with our experimental and theoretical results close to threshold. In the HF calculation of Starace *et al.* [25] up to 124 eV, the relatively large discrepancies between the length and velocity gauge results indicate the importance of including the coupling of the $[2p]$ continuum channels as noted by Henry [24]. The results of a recent R- matrix calculation given in the length gauge [28] exhibit surprising undulations in the branching ratios up to 200 eV, as is demonstrated, for example, by the significant difference in the calculated ratios at 40.8 and 95.0 eV (see Table II).

For photon energies below the $2s \rightarrow np$ autoionization energy region, our calculated and measured $[2p]$ branching

TABLE II. Comparison of experimental and theoretical $[2p]^2D$ to ^4S and ^2P to ^4S photoionization cross-section ratios for atomic oxygen. The experimental values of Refs. [9] and [20] are interpolated from their data. The velocity gauge calculations are indicated with square brackets.

$h\nu$	Experiment				Theory			
(eV)	This work	a	b	c,d	MCHF	R-matrix[e]	HF[f]	C-C[g]
					$^2D/^4S$			
19.9	1.22(10)	1.63(15)	1.58(16)		1.05[0.99]	1.39	1.44[1.13]	1.50[1.54]
21.22	1.37(12)[h]	1.56(19)	1.51(15)	1.57(14)[c]	1.14[1.10]	1.46	1.48[1.19]	1.54[1.59]
21.9	1.42(11)		1.48(15)		1.19[1.17]	1.50	1.50[1.22]	1.55[1.61]
23.9	1.53(12)		1.42(14)		1.25[1.24]	1.58	1.53[1.29]	1.56[1.64]
40.8	1.51(11)[h]			1.65(13)[d]	1.46[1.45]	1.71	1.50[1.42]	1.33[1.62]
95.0	1.42(6)[i]				1.40[1.39]	1.14	1.17[1.26]	1.25[1.27]
					$^2P/^4S$			
19.9	0.40(6)	0.88(8)			0.56[0.51]	0.61	0.88[0.59]	0.86[0.81]
21.22	0.47(7)[h]	0.97(15)		0.82(7)[c]	0.64[0.61]	0.68	0.95[0.66]	0.92[0.86]
21.9	0.55(6)				0.68[0.66]	0.72	0.96[0.69]	0.93[0.87]
23.9	0.68(7)				0.74[0.73]	0.79	1.00[0.75]	0.97[0.92]
40.8	0.80(8)[h]			0.92(13)[d]	0.88[0.94]	0.99	0.99[0.91]	0.85[0.89]
95.0	0.81(6)[i]				0.77[0.85]	0.63	0.69[0.76]	0.75[0.75]

[a]Reference [20].
[b]Reference [9].
[c]Reference [19].
[d]Reference [21].
[e]Reference [28].
[f]Reference [25].
[g]Reference [24]; values extracted from plot.
[h]Interpolated.
[i]Averaged between 80 and 110 eV.

ratios diverge from the relatively constant values obtained at high photon energy. Our experimental ^2D to ^4S ratio increases with increasing photon energy whereas the interpolated values from the measurements of van der Meulen *et al.* [9] indicate a slight decrease in this ratio with increasing photon energy over this energy range. At 19.9 eV our measured value is considerably below those of van der Meulen *et al.* and Hussein *et al.* [20]. Indeed, Hussein *et al.* observed no significant deviation in the ^2D to ^4S ratio down to a photon energy of 18.79 eV. In an experiment which used He I radiation at 21.22 eV, Samson and Petrovsky measured a ^2D to ^4S ratio of 1.57(14) [19] which lies above the ratio of 1.37(12) interpolated from our data. In this energy range close to threshold, the MCHF ^2D to ^4S ratios lie below the experimental and other theoretical values. Calculations predict, however, a rise in this ratio as the photon energy increases from 19.9 to 23.9 eV with which only the present measurement agrees. The deviation between the MCHF and HF results close to threshold is indicative of the importance of including electron correlation for such calculations which involve low-kinetic-energy electrons.

An increase in the ^2P to ^4S ratio with increasing photon energy is also seen in the present experimental results and the various calculations between 19.9 and 23.9 eV, with the experimental results generally lying lower than the calculated values and displaying a much steeper rise in the ratio. At 19.9 eV our measured value for the ^2P to ^4S ratio is over a factor of 2 smaller than that measured by Hussein *et al.* Over the photon energy range from 0.16 eV above the ^2P threshold at 18.79 eV to $h\nu = 21.38$ eV, Hussein *et al.* measured values ranging from 0.82 to 1.10 with no clear photon energy dependence. At 21.22 eV, Samson and Petrovsky measured a value of 0.82(7) for the ^2P to ^4S ratio, which also lies significantly above a value of 0.47(7) interpolated from our experimental results. The R-matrix results agree rather well with the MCHF calculation in this energy region, with the MCHF calculation giving a value of 0.64 (0.61) in the length (velocity) gauge at 21.22 eV.

Although the determination of the branching ratios close to the ionization thresholds was not a primary goal of our study, the comparison in Table II of the low-energy data from various sources demonstrates that the different experimental and theoretical results often display considerable variances in this range. This is not surprising, as this region is expected to be most sensitive to the details of electron correlation and dynamics in the calculation, and the experiment is more susceptible to the difficulties associated with detection of low-energy electrons. Our experimental data, while in fair agreement with the MCHF results, follow the same trend as the calculation. It is evident from the intercomparison of all available results that an extensive effort will be required for a definitive establishment of the near-threshold behavior.

As shown in Table II, our measured and calculated ^2D to ^4S and ^2P to ^4S ratios agree within the errors with those of Dehmer and Dehmer at 40.8 eV [21]. A close-coupling calculation at this photon energy, which includes some configuration interaction and the coupling of the $[2s]^4P$ and ^2P continuum channels in addition to the $[2p]$ continua, predicts a ^2P cross section larger than the ^2D cross section [26], which disagrees with both of these experimental results, our MCHF calculation, and other calculations

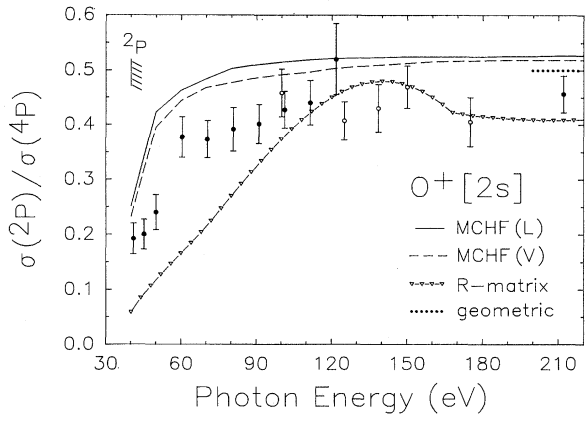

FIG. 5. Comparison of experimental and theoretical atomic oxygen $[2s]^2P$ to ^4P cross-section ratios. The MCHF length and velocity gauge results are indicated by solid and dashed lines, respectively. The geometric values are given by a dotted line. Also shown are R-matrix results of Bell and Stafford [28] (triangles). The measurements made on the Mark V monochromator are indicated by open symbols.

[24,25,28], as pointed out by Bell and Stafford [28]. The average experimental ^2D to ^4S and ^2P to ^4S ratios between 80 and 110 eV are 1.42(6) and 0.81(6), respectively, and compare excellently with the corresponding MCHF results (see Table II).

B. $[2s]$ multiplet cross-section ratios

In Fig. 5 the measured $O^+[2s]^2P$ to $[2s]^4P$ cross-section ratios for photon energies from close to the ^2P threshold to 212 eV are compared with the MCHF results, the R-matrix results of Bell and Stafford [28], and with the geometric ratio, which is 0.5. The principle contributions to the errors are the uncertainty in the transmission function correction and statistical uncertainty. The transmission function correction to the raw ratios, however, is less than 4% for photon energies above 130 eV and is well calibrated by the Ne $[2s]$ to $[2p]$ intensity ratios. A sharp rise in the $O^+[2s]^2P$ cross section relative to the $[2s]^4P$ cross section within $\approx$ 25 eV of the ^2P threshold is found in both the experimental and theoretical results and stems from the relatively large difference in binding energy of the $[2s]$ ionic states. The experimental asymptotic value of 0.46(5) lies below the geometric and the MCHF high-photon-energy ratios. The R-matrix results display a more gradual rise in this ratio, reaching a broad maximum at approximately 140 eV and decreasing to $\approx$0.41 at 200 eV.

C. Subshell cross-section ratios

The experimental $[2s]$ to $[2p]$ cross-section ratios between photon energies of 35 and 212 eV are compared with the MCHF calculation and a previous HS calculation [27] in Fig. 6. As was the case for the $[2p]$ branching ratios, the dominant contribution to the errors for $h\nu >$ 110 eV is the uncertainty in the molecular background underlying the $[2p]^2D$ and ^2P peaks. The experimental values for photon energies above 45 eV lie lower than the calculated ratios, but

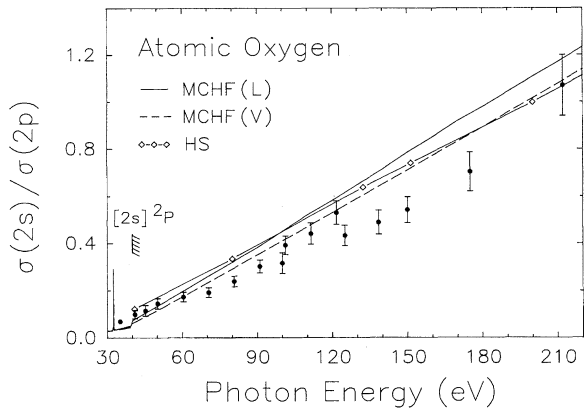

FIG. 6. Comparison of experimental and theoretical atomic oxygen $[2s]$ to $[2p]$ cross-section ratios. Results of a Hartree-Slater calculation [27] are represented by open diamonds.

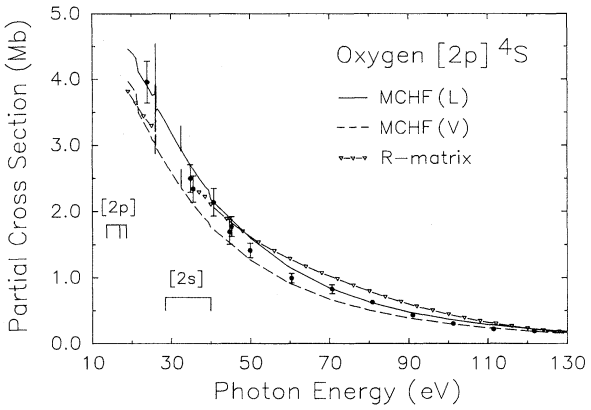

FIG. 7. Comparison of experimental and theoretical atomic oxygen $[2p]^4S$ partial photoionization cross sections. The experimental data represented by the filled circles are normalized to 2.36 Mb at 37.6 eV. The theoretical results include our MCHF length and velocity gauge calculations (solid and dashed lines, respectively) and a recent R-matrix calculation [28] (open inverted triangles). Energies of the multiplet components are indicated by connected vertical lines.

both the experimental and theoretical values display a nearly linear rise in the ratio up to the highest recorded photon energy. The MCHF calculation has a slightly steeper slope than the HS results over this energy range. A similar, approximately linear, rise with photon energy in the $[2s]$ to $[2p]$ cross-section ratio has been observed for neon [7,36,37]. The slope of the linear rise of the ratio for neon, reaching a value of 1.0 at $h\nu \approx 625$ eV, is lower than that for oxygen by roughly a factor of 3.4 . The steeper slope in oxygen is only partly due to the smaller number of $2p$ electrons.

D. Partial and total cross sections

The relative partial photoionization cross section for the $O^+[2p]^4S$ state was measured at selected photon energies between 24 and 122 eV. The measurement was put on an absolute scale by normalizing the sum of our partial cross sections to the absolute O^+ total cross-section measurements of Angel and Samson [29] in the photon energy region from 35 to 41 eV; we match our data at 37.6 eV to $\sigma_{tot} = 8.6$ Mb for the total O^+ cross section. Autoionization resonances occurring in this range were of no concern since experimental observation has shown these features to be small [29]. Using the measured $\sigma[2s]/\sigma[2p]$ ratios and the $[2p]$ branching ratios, which are given in Table I and Figs. 3 and 6, the corresponding partial cross section for the $O^+[2s]^4S$ state amounts to 2.36(12) Mb at 37.6 eV. This value serves as the reference point for both the partial and total cross sections presented in the following over the photon energy range from 24 to 122 eV. The uncertainties of the data include those in the cross-section ratios for the $2s$ and $2p$ subshells, those in the branching ratios, and the uncertainty in the transmission function of the monochromator. The quoted uncertainty of 4.4% in the absolute cross-section measurement of Angel and Samson [29] is not included here.

In Fig. 7 we compare the measured $[2p]^4S$ partial cross section with our MCHF results throughout and the R-matrix results of Bell and Stafford [28] in the energy region undisturbed by resonance processes. The measured values are seen to agree well with the MCHF results in the region of *continuous* photoabsorption. At the lower photon energies the experimental data are in better accord with the results in the length gauge, while at the higher energies, $h\nu > 100$ eV, the accord is better with the results in the velocity gauge. Over the entire range the MCHF length results are 15–20 % higher than those of the MCHF velocity gauge. The R-matrix predictions, presented in the length gauge only [28], lie within 20% of the experimental and the MCHF length results, although this partial cross section decreases less steeply with energy in the R-matrix formulation than in the MCHF calculation.

While a partial cross section such as shown in Fig. 7 provides a critical analysis of the photoionization process, the total cross section affords an overall view of the phenomenon. Figure 8 shows the measured total cross section on an absolute scale as the sum of the partial cross sections for single-electron emission from the $2p$ and $2s$ subshells. (Specific values are given in Table III.) These data are compared with the direct measurement of the O^+ ion current by Angel and Samson [29]. There is a good agreement for the cross-section *dependence* of these two data sets that have been obtained by different methods. The ion yield and electron spectrometry measurements should in principle differ above 40 eV due to the inclusion of excited states of O^+ in the ion yield measurement. The contribution of the two O^+ satellites seen in Fig. 4 at binding energies of 42.30 and 52.80 eV to the total O^+ cross section, however, is only 2.5(1.2)% at 212 eV. The satellite with a binding of 26.8 eV may arise from the $O_2\,{}^1\Delta_g \rightarrow {}^2\Delta_u$ transition calculated by Jonathan *et al.* to have a vertical ionization energy of 26.50 eV [45].

The MCHF calculation for the sum of the $[2p]$ and $[2s]$ cross sections agrees satisfactorily with the experimental results on the absolute scale, which is based on the measurement of Angel and Samson. As was the case for the $[2p]^4S$ partial cross section, the length gauge gives better agreement at the lower energies and the velocity gauge at the

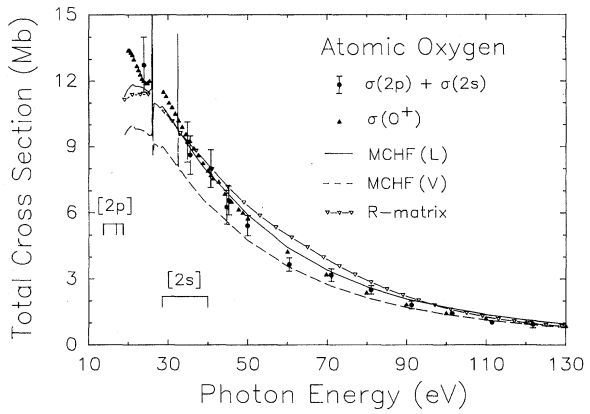

FIG. 8. Comparison of experimental and theoretical atomic oxygen photoionization cross sections. Our data (solid circles) are normalized to $\sigma = 8.6$ Mb at $h\nu = 37.6$ eV. Solid triangles are absolute ion yield measurements [19]. Results of the R-matrix calculation are given by the open inverted triangles. Connected vertical lines indicate the energies of the multiplet components.

higher energies. The R-matrix results, given in the length gauge, agree well with the corresponding MCHF results, apart from the less steep energy dependence, as is seen even more distinctly in the $[2p]^4S$ cross section. We note that, in addition to the recent R-matrix calculation [28], there have been a number of other measurements and calculations of the total photoionization cross section of atomic oxygen which are not included here but have been previously intercompared [22,23,28,29].

V. CONCLUSIONS

The valence shell photoionization branching ratios of atomic oxygen have been measured at the LS term level with synchrotron radiation-based electron spectrometry and calculated using the MCHF method for photon energies from close to threshold to 212 eV in the regions of continuous photoabsorption. The experimental $[2p]({}^4S,{}^2D,{}^2P)$ branching ratios compare well with those from the MCHF calculation over the entire energy range, except for the very lowest energies, and are close to the geometric values at photon energies above 90 eV. The MCHF ratios are essentially constant above 90 eV. The results of the branching ratios indicate that the partitioning of the $2p$ subshell cross section into the multiplet components is governed primarily by geometric considerations provided the photon energies are greater than about five times the ionization threshold energies. Closer to threshold the experimental and theoretical branching ratios deviate from the constant values, indicating the presence of dynamic and kinetic effects. Previous measurements of these ratios, which have been performed only up to 41 eV, are at variance with our data in some cases. For the $[2s]^2P$ to $[2s]^4P$ cross-section ratio we observe a gradual rise of the ratio until a fairly constant value is reached in both the experiment and the MCHF calculation at an energy that is roughly three times the ${}^2P$ binding energy. The theoretical value at high energy is slightly higher than the geometric value, while the experimental value is slightly lower. The experimental partial and total cross sections, placed on an absolute scale, as well as the $[2s]$ to $[2p]$ subshell cross-section ratio, are seen to be in good agreement with the MCHF results and the results of an R-matrix calculation in the 24–122-eV range covered by our work.

In summary, this study of the oxygen atom provides a base-line result for the photoionization process in a simple open-shell atom over a broad photon energy range. Specifically, this work yields partial and total photoionization cross sections in the continuous region of absorption for the outer subshells of the O atom. At high photon energies the partitioning of a subshell cross section into its multiplet components is shown to be dominated by geometric effects, that is, by the angular momentum coupling of the final ionic states. We may infer from the present results that the geometric values should be a good approximation for the branching ratios in other open-shell atoms for excitation energies somewhat above the pertinent ionization thresholds and outside regions of autoionization resonances and Cooper minima. In the general case, the effect of these features, as well as the influence of two-electron interactions leading to correlation satellites, must await further detailed examination.

TABLE III. Measured photoionization cross section σ for the sum of the main $[2p]$ and $[2s]$ photolines, normalized to 8.6 Mb at 37.6 eV.

$h\nu$ (eV)	σ (Mb)
23.9	12.7(1.3)
34.8	9.21(91)
35.5	8.62(85)
40.7	8.00(84)
44.7	6.25(76)
45.2	6.56(66)
49.9	5.42(55)
60.4	3.66(31)
70.5	3.17(29)
80.8	2.50(20)
91.0	1.81(18)
101.2	1.43(12)
111.4	1.03(2)
121.7	0.93(17)

ACKNOWLEDGMENTS

This work was supported in part by the National Science Foundation under Grant No. PHY-9207634 and in part by U.S. Department of Energy, Basic Energy Sciences, under Contract No. DE-AC05-84-OR21400 with Martin Marietta Energy Systems, Inc. The Synchrotron Radiation Center is supported by the National Science Foundation under Grant No. DMR-9212658. S.J.S. thanks the Alexander von Humboldt Foundation for support during the preparation of the manuscript and V. Schmidt for his hospitality at the Universität Freiburg. J.J.M. also acknowledges support from CONACYT under Contract No. 6140105-4400-G000-9-09. We are indebted to Dr. Bell and Dr. Stafford for providing us with the numerical output of their calculations.

[1] A.F. Starace, in *Corpuscles and Radiation in Matter*, edited by W. Mehlhorn, Handbuch der Physik Vol. 31 (Springer Verlag, Berlin, 1982), p. 1.
[2] H.P. Kelly, Phys. Scr. **T17**, 109 (1987).
[3] M. Ya Amusia, *Atomic Photoeffect* (Plenum Press, New York, 1990).
[4] V. Schmidt, Rep. Prog. Phys. **55**, 1483 (1992).
[5] M.O. Krause, Phys. Rev. **177**, 151 (1969).
[6] J.W. Cooper and S.T. Manson, Phys. Rev. **177**, 157 (1969).
[7] F. Wuilleumier and M.O. Krause, Phys. Rev. A **10**, 242 (1974).
[8] G.L. Goodman and J. Berkowitz, J. Chem. Phys. **94**, 321 (1991).
[9] P. van der Meulen, M.O. Krause, and C.A. de Lange, Phys. Rev. A **43**, 5997 (1991), and references therein.
[10] B. Sonntag and P. Zimmermann, Rep. Prog. Phys. **55**, 911 (1992), and references therein.
[11] M.O. Krause, C.D. Caldwell, S.B. Whitfield, C.A. de Lange, and P. van der Meulen, Phys. Rev. A **47**, 3015 (1993), and references therein.
[12] P.A. Cox and F.A. Orchard, Chem. Phys. Lett. **7**, 273 (1970).
[13] J. Schirmer, L.S. Cederbaum, and J. Kiessling, Phys. Rev. A **22**, 2696 (1980).
[14] Ch. Pan and A.F. Starace, Phys. Rev. A **47**, 295 (1993).
[15] K. Kimura, T. Yamazaki, and Y. Achiba, Chem. Phys. Lett. **58**, 104 (1978).
[16] J. Berkowitz and G.L. Goodman, J. Chem. Phys. **71**, 1754 (1979).
[17] P. van der Meulen, M.O. Krause, and C.A. de Lange, J. Phys. B **25**, 97 (1992).
[18] P. van der Meulen, M.O. Krause, C.D. Caldwell, S.B. Whitfield, and C.A. de Lange, Phys. Rev. A **46**, 2468 (1992).
[19] J.A.R. Samson and V.E. Petrovsky, Phys. Rev. A **9**, 2449 (1974).
[20] M.I.A. Hussein, D.M.P. Holland, K. Codling, P.R. Woodruff, and E. Ishiguro, J. Phys. B **18**, 2827 (1985).
[21] J.L. Dehmer and P.M. Dehmer, J. Chem. Phys. **67**, 1782 (1977).
[22] Y. Itikawa and A. Ichimura, J. Phys. Chem. Ref. Data **19**, 637 (1990).
[23] J.A. Fennelly and D.G. Torr, At. Data Nucl. Data Tables **51**, 321 (1992).
[24] R.J.W. Henry, Planet. Space Sci. **15**, 1747 (1967).
[25] A.F. Starace, S.T. Manson, and D.J. Kennedy, Phys. Rev. A **9**, 2453 (1974).
[26] A.K. Pradhan, Planet. Space Sci. **28**, 165 (1980).
[27] J.J. Yeh and I. Lindau, At. Data Nucl. Data Tables **32**, 1 (1985).
[28] K.L. Bell and R.P. Stafford, Planet. Space Sci. **40**, 1419 (1992).
[29] G.C. Angel and J.A.R. Samson, Phys. Rev. A **38**, 5578 (1988).
[30] C.D. Caldwell and M.O. Krause, Phys. Rev. A **47**, R759 (1993).
[31] H.P. Saha, Phys. Rev. A **49**, 894 (1994).
[32] C.D. Caldwell, S.J. Schaphorst, M.O. Krause, and J. Jiménez-Mier, J. Electron Spectrosc. Relat. Phenom. **67**, 243 (1994).
[33] M.O. Krause, T.A. Carlson, and A. Fahlman, Phys. Rev. A **30**, 1316 (1984).
[34] T.A. Calcott, E.T. Arakawa, and D.L. Ederer, Jpn. J. Appl. Phys. **17** (Suppl. 17-2), 149 (1978).
[35] M. Larsson, P. Baltzer, S. Svensson, B. Wannberg, N. Mårtensson, A. Naves de Brito, N. Correia, M.P. Keane, M. Carlsson-Göthe, and L. Karlsson, J. Phys. B **23**, 1175 (1990).
[36] F. Wuilleumier and M.O. Krause, J. Electron Spectrosc. Relat. Phenom. **15**, 15 (1979).
[37] A.D.O. Bawagan, B.J. Olsson, K.H. Tan, J.M. Chen, and B.X. Yang, Chem. Phys. **164**, 283 (1992).
[38] G.V. Marr and J.B. West, At. Data Nucl. Data Tables **18**, 497 (1976).
[39] J.A.R. Samson, J.L. Gardner, and G.N. Haddad, J. Electron Spectrosc. Relat. Phenom. **12**, 281 (1977).
[40] H.P. Saha, Phys. Rev. A **39**, 2456 (1989).
[41] S. Southworth, C.M. Truesdale, P.H. Kobrin, D.W. Lindle, W.D. Brewer, and D.A. Shirley, J. Chem. Phys. **76**, 143 (1982).
[42] Y. Iida, F. Carnovale, S. Davial, and C.E. Brion, Chem. Phys. **105**, 211 (1986).
[43] H.-J. Freund, H. Kossmann, and V. Schmidt, Chem. Phys. Lett. **137**, 425 (1987).
[44] J.W. Gallagher, C.E. Brion, J.A.R. Samson, P.W. Langhoff, JILA Data Center Report No. 32 (unpublished).
[45] N. Jonathan, A. Morris, M. Okuda, K.J. Ross, and D.J. Smith, J. Chem. Soc. Faraday Trans. 2 **70**, 1810 (1974).
[46] H. van Lonkhuyzen and C.A. de Lange, J. Electron Spectrosc. Relat. Phenom. **27**, 255 (1982); H. van Lonkhuyzen, Ph.D. thesis, Free University Amsterdam, The Netherlands (1984).
[47] W.J. van der Meer, P. van der Meulen, M. Volmer, and C.A. de Lange, Chem. Phys. **126**, 385 (1988).
[48] K. Pearson, Biometrika **16**, 157 (1924).